CHAPTER

2

Fundamentals

Wenting Sun[a], *Subith Vasu*[b], *and Matthew S. Blais*[c]

[a]Georgia Institute of Technology, Atlanta, GA, United States [b]University of Central Florida, Orlando, FL, United States [c]Southwest Research Institute, San Antonio, TX, United States

2.1 Physical and chemical properties of hydrogen

Hydrogen (or dihydrogen molecule, H_2) has a long history of being considered as a fuel. Compared to its hydrocarbon counterparts, hydrogen has very unique physical and chemical properties. This chapter was prepared for readers who would like to get a quick overview of the characteristics of hydrogen combustion-related phenomena. If the readers wish to learn the general fundamentals or underlying detailed kinetics/physics, they are referred to the references cited in this chapter.

Hydrogen is a colorless and odorless gas. It is almost insoluble in water. The melting point of hydrogen is −259.19°C, and the boiling point is −252.76°C (Wiberg et al., 2001). The critical temperature and pressure of hydrogen are 32.9 K and 1.29 MPa, respectively (Wiberg et al., 2001). It is worth noting that a hydrogen mixture could have a critical pressure much higher than the critical pressure of pure hydrogen (Karimi et al., 2021).

Hydrogen is the lightest element, followed by helium (He). The molecular weight of H_2 is 2.01594 g/mol. Since hydrogen has the lowest molecular mass, it has a low density, high heat capacity per mass, and very high diffusivity. These unique physical properties together with its also unique chemical properties make hydrogen combustion vastly different from the combustion of hydrocarbons. Hydrogen is extremely buoyant and tends to cause stratification, creating a concentration gradient unless mechanically mixed or allowed to sit in an enclosed space for extended periods. As a result, 10% measured at floor level when ignited can accelerate upward and reach the point of deflagration to detonation transition (DDT, covered in depth in chapter 7 under Safety). Details of hydrogen combustion properties will be discussed in the following sections of this chapter.

The bond energy of H—H is about 432 kJ/mol, which is similar to C—H bond energy (~413 kJ/mol). Hydrogen flammability is 4%–75% (fuel volume fraction) in the air (Glassman et al., 2014) at 25°C and atmospheric pressure. These values correspond to equivalence ratios 0.1 and 7.14, respectively. As a comparison, the flammability of hydrogen

https://doi.org/10.1016/B978-0-323-90394-3.00015-1

changes from 4% to 94% (fuel volume fraction) in pure oxygen (Glassman et al., 2014). The widely-used flammability values were obtained from experiments using the "tube method" in 1965 by the US Bureau of Mines (Zabetakis, 1965). In this method, a vertical tube with approximately 50 mm diameter by 1.2 m long was used. A flame was initiated at the bottom of the tube and propagated the length of the tube. A mixture that sustained the flame was said to be flammable. Therefore, flammability limits define the lean and rich fuel/oxidizer ratio beyond which no flame will propagate at a given temperature and pressure condition (Glassman et al., 2014). The quenching distance for stoichiometric hydrogen/air mixture is 0.64 mm, and the minimum ignition energy of hydrogen/air mixture is approximately 2×10^{-5} J (Barnett and Hibbard, 1958). While databases or handbooks may provide a specific auto-ignition temperature or flammability range, it is important to remember that those specific values could be affected by pressure and temperature conditions. Protocols should be specified on how these values were obtained.

The global, one-step oxidation reaction of hydrogen with air is

$$2H_2 + O_2 + 3.76N_2 \rightarrow 2H_2O + 3.76N_2$$

The heat of combustion of hydrogen is 285.8 kJ/mol or 141.8 MJ/kg (higher heating value at the standard conditions) (Haynes, 2014). Hydrogen is highly flammable and explosive, owing to its broad range of flammability. The low molecular weight of hydrogen makes its speed of sound high, therefore, the strong shock could be introduced if there was a high-pressure hydrogen leak. The auto-ignition temperature is relatively low, approximately between 500°C and 570°C (U.S. C. Guard, 1999; Colonna, 2010). Such a high-pressure hydrogen leak could subsequently promote auto-ignition and then an explosion. Extra caution is needed when working on hydrogen combustion.

Another unique feature of hydrogen flame is its significantly weaker chemiluminescence than comparable hydrocarbon flames, which is almost invisible to naked eyes. This is in contrast with natural gas flames which are blue and flames using large hydrocarbons with orange-colored flames owing to soot formation. The emission band head of hydrogen flame is in the ultra-violet (UV) region near 310 nm which is invisible to human eyes. Emissions in the visible region extending from 400 to 750 nm are very weak for hydrogen flames. Usually, a reduced light level is required to make a hydrogen flame visible (Schefer et al., 2009). Fig. 2.1 shows flame images of hydrogen (left) and propane (right) taken by an ordinary digital camera showing the entirely invisible features of a hydrogen flame (Okino et al., 2017). As a comparison, Fig. 2.2 shows a hydrogen flame (Schefer et al., 2002) with a reduced background light level and long exposure time.

The application of hydrogen combustion requires extreme carefulness. Hydrogen has been demonstrated to DDT when at concentrations of 28% in normal air, when enriched oxygen is present at concentrations as low as 18%, in highly turbulent mixing environments, in a gradient concentration where ignition is at 8% and an upward gradient is present giving rise to 28%, or where localized entrapment causes hydrogen-enriched environments. Many of these factors are caused by the high buoyancy of hydrogen; a cubic meter of hydrogen can lift 1.1 kg of weight. This buoyance creates significant concentration gradients from floor to ceiling. The measurement of hydrogen leaks should always be performed at the highest point the leak might affect unless there is an entrapment location in the path. For this reason, the introduction of hydrogen should be from the top of the apparatus, and all fittings and possible leak points should have a clear upward path to an exhaust system. Even if the path is free from

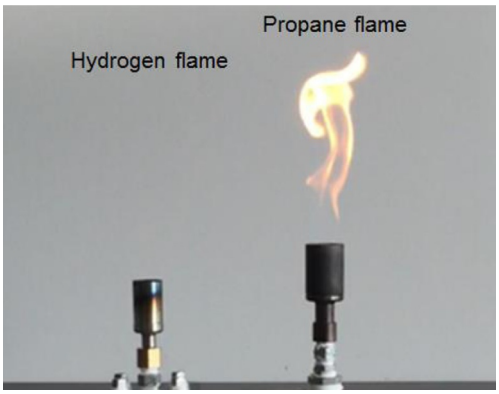

FIG. 2.1 Flame images of hydrogen *(left)* and propane *(right)* taken by an ordinary digital camera (Okino et al., 2017).

FIG. 2.2 Flame luminosity photograph in NASA Glenn hydrogen burner with 0.6 s exposure time (Schefer et al., 2002).

entrapment clutter from steel members or other structures above, a leak can create turbulence in the upward burning fire that leads to a DDT. This can occur with as low as 12% hydrogen in normal air. This particular example was a case of the flame going against the concentration gradient and finding a localized fuel-rich environment. Cluttered environments, structural elements in the burn path, and entrapment are all hazardous conditions in hydrogen leak environments that have led to unexpected detonations.

For these reasons, designing hydrogen-driven power generation, engines or turbines should focus on delivering the hydrogen in the upper half of the system with little to no structural members above the injection points. This allows for buoyancy to remove hydrogen

naturally from the machinery/potential ignition point. Vents at the peak or top of an enclosure will also prevent a flammable environment build-up, increasing safety.

2.2 Fundamental hydrogen reaction kinetics

The purpose of this section is to outline the elementary reaction steps involved in hydrogen-related combustion systems. The chemical kinetics are generally complex and evolving even for hydrogen, which is considered the simplest fuel in molecular structure. For an in-depth discussion of hydrogen kinetics, the reader is referred to the original literature (Burke et al., 2021; ÓConaire et al., 2004; Kéromnès et al., 2013; Konnov, 2019).

2.2.1 Explosion limits of hydrogen and oxidation kinetics of hydrogen

Hydrogen kinetics has been widely studied due to the importance of hydrogen in applications such as rocket propulsion and its crucial role in general chemical kinetics. Typical chemical kinetic models of hydrogen carbons have hierarchical and modular structures as illustrated in Fig. 2.3. Hydrogen could be produced as an intermediate species during the oxidation process of hydrocarbons, such as methane (CH_4). So hydrogen kinetics is essentially part of any hydrocarbon kinetic model and moist carbon monoxide kinetic model.

Reactions in combustion systems can be categorized into chain initiation reactions, chain branching reactions, chain propagating reactions, and chain-terminating reactions. In chain initiation reactions, a radical is produced without a radical reactant such as

$$H_2 + M \rightarrow H + H + M \qquad \text{(i)}$$

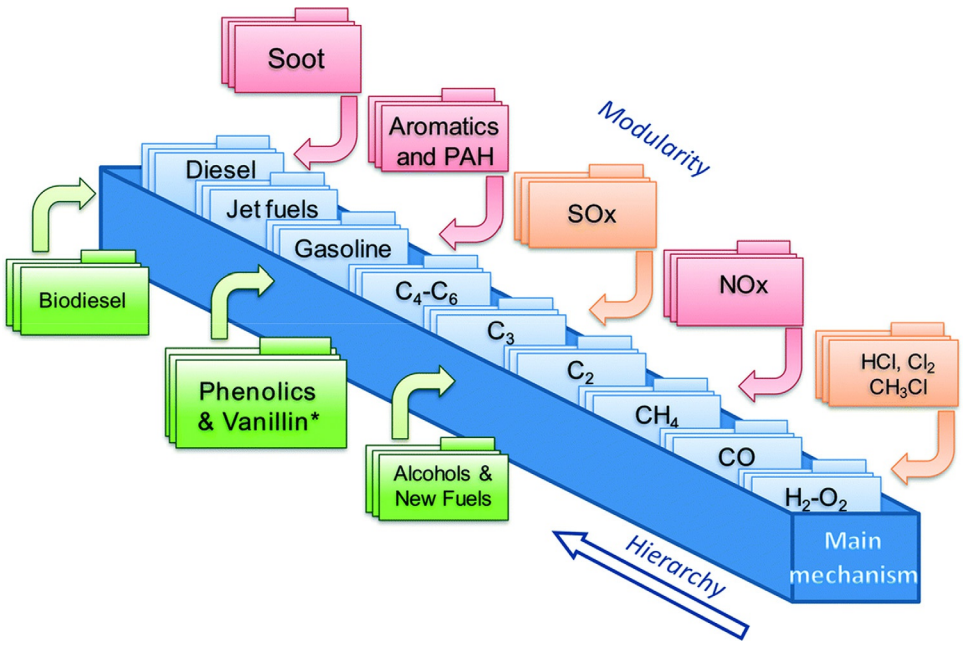

FIG. 2.3 Schematic view of kinetic model with the hierarchical and modular nature (Pelucchi et al., 2019).

$$H_2 + O_2 \rightarrow HO_2 + H \quad \text{(ii)}$$

where M represents a third body collider that provides (or takes away) the energy necessary to break the chemical bond (or stabilize the product through combination). The reaction (i) requires the break of the hydrogen chemical bond, so a very high temperature is required. The reaction (ii) has lower activation energy than reaction (i), so it is more active at lower temperature conditions.

In chain branching reactions, there is a net radical production, such as

$$H + O_2 \rightarrow OH + O \quad \text{(iii)}$$

$$O + H_2 \rightarrow H + OH \quad \text{(iv)}$$

$$O + H_2O \rightarrow OH + OH \quad \text{(v)}$$

In a chain-propagating reaction, the reaction consumes and produces the same number of radicals, such as

$$H_2 + OH \rightarrow H_2O + H \quad \text{(vi)}$$

In chain-terminating reactions, there is net destruction of radicals, such as.

$$H + H + M \rightarrow H_2 + M \quad \text{(vii)}$$

$$O + O + M \rightarrow O_2 + M \quad \text{(viii)}$$

$$H + O + M \rightarrow OH + M \quad \text{(ix)}$$

$$H + OH + M \rightarrow H_2O + M \quad \text{(x)}$$

Chain termination reactions could also include a reactor wall effect: H/OH ➔ wall destruction.

Almost all reactions are temperature and pressure-dependent. The global reaction $2H_2 + O_2 \rightarrow 2H_2O$ is the lump sum, competing for the effect of all underlying elementary reactions. The explosion limits of hydrogen can demonstrate such competing effects. To fully explain the explosion limits of hydrogen, we also need to include reactions involving HO_2, the hydroperoxy radical, and H_2O_2, hydrogen peroxide.

$$H + O_2 + M \rightarrow HO_2 + M \quad \text{(xi)}$$

$$HO_2 + H \rightarrow OH + OH \quad \text{(xii)}$$

$$HO_2 + H \rightarrow H_2O + O \quad \text{(xiii)}$$

$$HO_2 + O \rightarrow O_2 + OH \quad \text{(xiv)}$$

$$HO_2 + HO_2 \rightarrow H_2O_2 + O_2 \quad \text{(xv)}$$

$$HO_2 + H_2 \rightarrow H_2O_2 + H \quad \text{(xvi)}$$

$$H_2O_2 + OH \rightarrow H_2O + HO_2 \quad \text{(xvii)}$$

$$H_2O_2 + H \rightarrow H_2O + OH \quad \text{(xviii)}$$

$$H_2O_2 + H \rightarrow HO_2 + H_2 \quad \text{(xix)}$$

$$H_2O_2 + M \rightarrow OH + OH + M \quad \text{(xx)}$$

Depending on the temperature and pressure conditions, HO_2 and H_2O_2 could be considered relatively stable species or chemically active species in explaining hydrogen explosion limits.

Fig. 2.4 shows the explosion limits of a stoichiometric hydrogen/oxygen mixture in a KCl-coated vessel with a 7.4 cm diameter. The temperatures and pressures correspond to the initial charging conditions of the spherical vessel containing the reactants. As shown in Fig. 2.4, there are distinct regions where the mixture will and will not explode. It can also be observed that there is no significant reaction progress below approximately 675 K, and that above 850 K explosion occurs spontaneously. Within this temperature regime, three explosion limits exist. Explosion limits are not flammability limits. Explosion limits are the pressure-temperature boundaries for a specific fuel/oxidizer mixture that separates the region of slow and fast reactions (Glassman et al., 2014).

To understand the explosion behavior, we can follow a specific vertical line, e.g., 500°C, starting from the lowest pressure upwards to the highest pressure shown in Fig. 2.4. There is no explosion in the regime below approximately 1.5 mmHg (below the first explosion limit). This is because free radicals produced in the initiation step (ii) and chain branching/propagating steps (iii)–(vi) are destroyed/quenched by the wall of the reactor, which is a chain termination process. Without the radical pool build-up process, the explosion will not occur. The wall reactions are not explicitly included in gas-phase chemical kinetic models, because they are not gas-phase reactions.

The mixture explodes if the mixture pressure is raised to above 1.5 mmHg (above the first explosion limit but below the second explosion limit). With increased pressure, the reaction rates increase, and the diffusion of radicals to the wall slows down. At this condition, the radical production process (iii)–(vi) prevails over the radical destruction on the reactor wall.

If the reactor pressure is further raised to above 50 mmHg (above the second explosion limit but below the third explosion limit), the mixture ceases to be explosive. With the increase of pressure, the reaction rate of reaction (xi) increases geometrically and outpace the competition of H radical with a chain branching reaction (iii). At relatively low-temperature conditions, HO_2 is unreactive (metastable), so reaction (xi) is essentially a chain-terminating reaction. Therefore, HO_2 has enough time to diffuse to the reactor wall and is destroyed through heterogeneous surface reaction (HO_2 species combine on surfaces to form H_2O and O_2 (Glassman et al., 2014). In summary, reaction (iii) generally dominates at higher temperatures and lower pressures, while reaction (xi) will be more effective at higher pressures and lower temperatures.

The mixture is explosive again above the third explosion limit (approximately 3000 mmHg at 500°C). At these conditions, reaction (xvi) (together with xx), which could be considered a chain branching reaction, becomes significant, making the mixture explosive.

Through this brief discussion on the explosion limits of the H_2/O_2 system, it is clear that a comprehensive understanding of detailed chemistry is essential to develop a hydrogen combustion system. In the following sections, more phenomena related to hydrogen combustion will be discussed based on the mechanism discussed in this section.

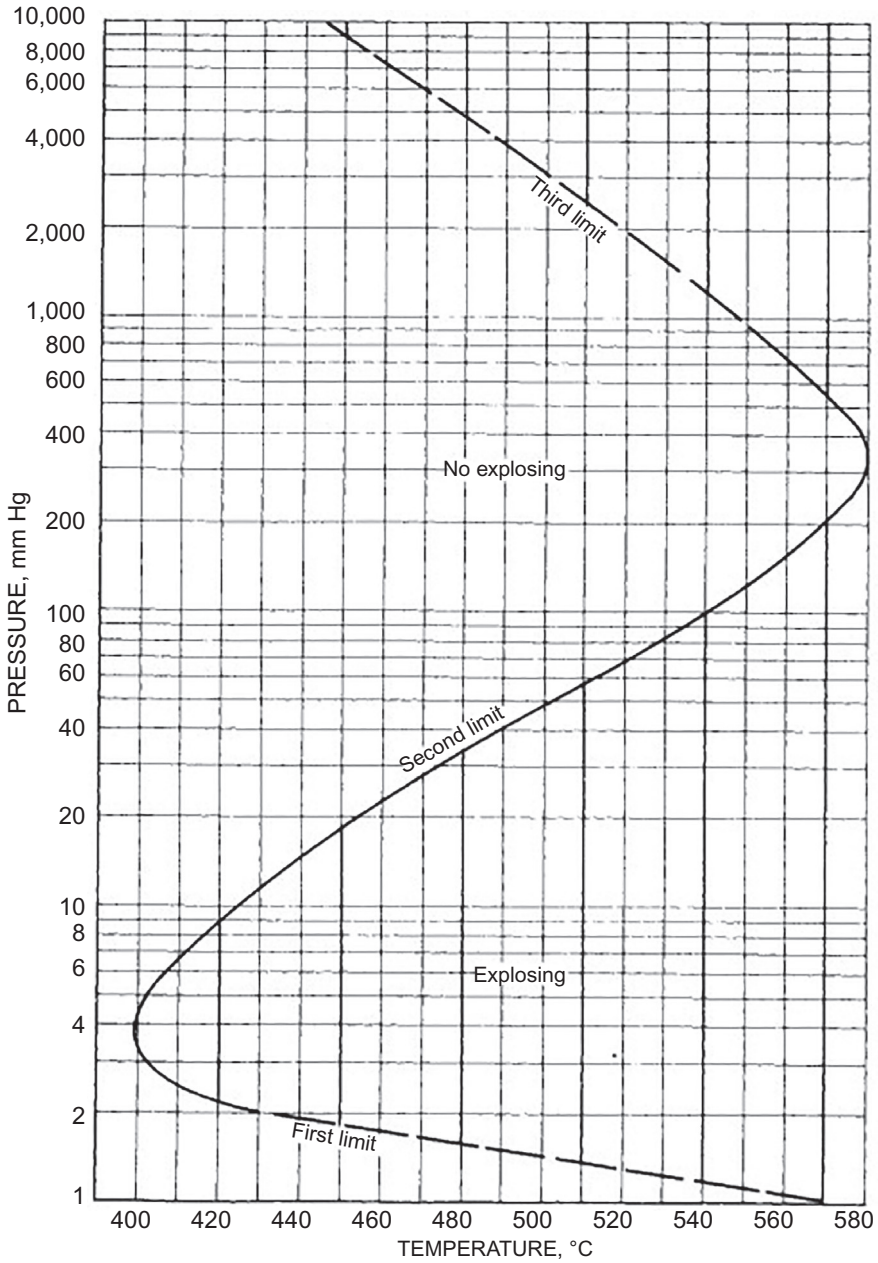

FIG. 2.4 Explosion limits of a stoichiometric hydrogen-oxygen mixture in a spherical KCl-coated vessel of 7.4 cm diameter. The first and third limits are partly extrapolated (Lewis and von Elbe, 1987).

2.2.2 Development of oxidation kinetics of hydrogen

The discussion on the explosion limits of hydrogen laid the foundation of hydrogen oxidation kinetics. Since the seminal work by Westbrook and Dryer (1984), hydrogen kinetic models have been improved significantly, and it is still evolving even now. In the past twenty years, a few hydrogen kinetic models were published, including models from ÓConaire et al. (2004), Hong et al. (2011), Burke et al. (2021), Kéromnès et al. (2013), Varga et al. (2015) and Konnov (2019). Most of the parameters were based on directly measured or theoretically calculated reaction rate coefficients in all of these models. Some of the rate parameters were tuned/optimized to improve the agreement with experimentally measured combustion properties such as autoignition delays, laminar flame speeds, and speciation.

During the development of hydrogen kinetic models in recent years, discrepancies between experiments and model predictions arise for high-pressure and/or dilute flame speeds. Most kinetic models failed to predict such a trend at high-pressure conditions. Fig. 2.5 from Burke et al. (2021) shows the comparison between experimentally measured laminar flame mass burning rates for H_2/O_2/He flames and predictions from different kinetic models. Discrepancies among experiments and model predictions become significant

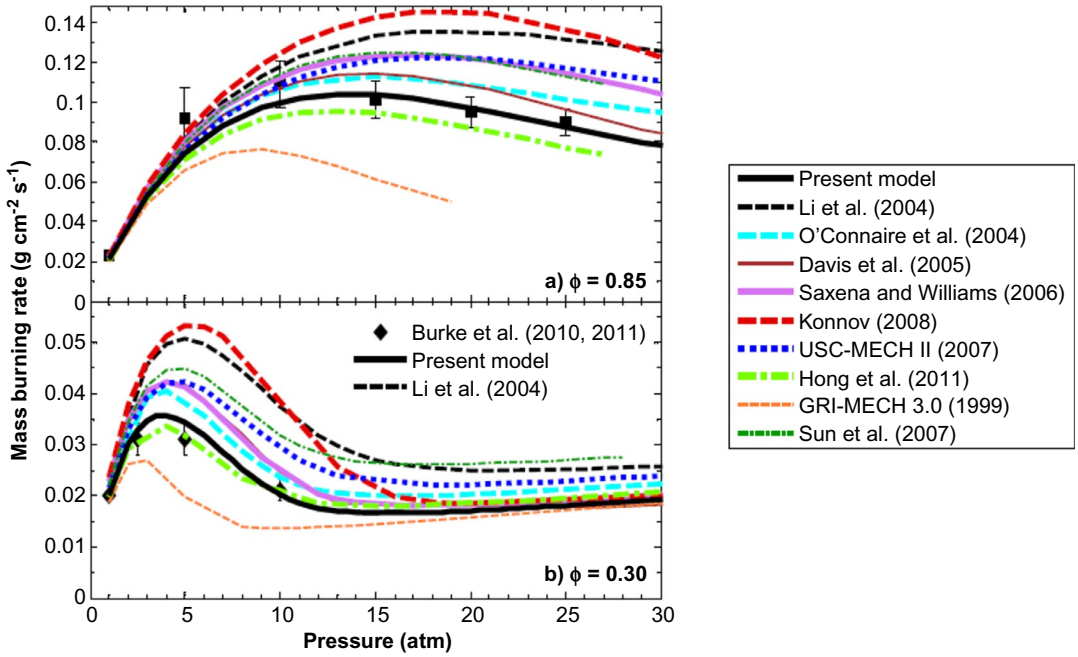

FIG. 2.5 Pressure dependence of the laminar flame mass burning rate for (A) H_2/O_2/He mixture of equivalence ratio 0.85 with dilution adjusted such that the adiabatic flame temperature is near 1600 K and (B) H_2/O_2/He mixture of equivalence ratio 0.30 with dilution adjusted such that the adiabatic flame temperature is near 1400 K. *Symbols* represent experimental data from Burke et al. (2010); *solid lines* are the present model and *dashed lines* the model of Li et al. (2004) predictions using the model of Davis et al. (2005), Konnov (2008), Sun et al. (2007), ÓConaire et al. (2004), Saxena and Williams (2006), GRI-MECH 3.0 (Smith et al., 2008), Hong et al. (2011), and USC-MECH II (Wang et al., 2007) are shown.

at high-pressure conditions. The model from Burke et al. (2021) (marked as "Present model" in Fig. 2.5) successfully predicted the trend of the experiments. So, the model from Burke et al. (2021) is used as an example for further discussion.

In general, the reaction kinetic model or mechanism describes the elementary reaction steps that occurred during the conversion of fuel/oxidizer to final products. In the combustion community, a uniform way of expressing the variation of reaction rates with temperature is adopted for modeling the kinetic process, which is the modified Arrhenius form:

$$k = AT^n \exp(-E_a/RT)$$

where k is the reaction rate coefficient (conventionally called the reaction rate constant). k depends on temperature T and an activation energy E_a, with a pre-exponential collision factor A. Table 2.1 shows the reactions included in the model developed by Burke et al. (2010). Over modest ranges of temperature, most binary elementary reactions follow the classical Arrhenius behavior and can be expressed into the single exponential term. However, significant non-Arrhenius behavior does exist over temperature ranges in combustion systems. Therefore, an additional correction of the rate coefficient with temperature must be included. For example, in Table 2.1, for reaction (2) $O+H_2=H+OH$, duplicate reactions are claimed. The actual reaction rate of reaction (2) is the summation of the reaction rates from these two duplicate reactions. The third body collision efficiency ε, has different values for different species. In a combustion environment, high concentrations of different species could exist simultaneously, so different species' third body collision efficiency plays an important role in a kinetic model. In general, H_2O and CO_2 molecules have higher, third body collision efficiencies, because they are more effective in taking away (or providing) additional energy for the reactions. In calculating reaction rates involving a third body collider with non-unity third body collision efficiency, the reaction rate constant is calculated by the revised Arrhenius expression multiplying the third body collision efficiency (weighted average).

Calculation of reaction rates for reactions (9) and (15) in Table 2.1 involves different pressure dependence. For such reactions, starting from the high-pressure limit, the rate coefficient decreases with decreasing third body concentration [M], and the corresponding representation of the reaction rate constant as a function of [M] is termed as the "falloff" curve of the reaction. In general, the pressure dependence of these reactions could be described by the Lindemann-Hinshelwood reaction scheme and calculated using the classical Troe formalism (Atkinson et al., 2004). The parameters for Troe formalism for reactions (9) and (15) in Table 2.1 are provided below each reaction in the table.

During the development of the kinetic model presented in Table 2.1, a key finding and improvement is the importance of the rate constants' temperature and pressure dependence for HO_2 formation and consumption reactions. This is particularly important on the predictability of the kinetic model at high pressure and low-temperature conditions.

By the time of completion of this chapter, the most recent kinetic model published was by Konnov (2019). In the updated Konnov model, chemically termolecular reactions (Klippenstein, 2017; Burke and Klippenstein, 2017), $H+O_2+R$ (R=H, O or OH) may significantly affect kinetic pathways in the conditions of high concentrations of H atoms and other radicals, are included. Together with the new transport database from Jasper et al. (2014), the updated H_2 kinetic model reportedly accurately reproduces burning velocities of H_2+air flames both in lean and rich mixtures within the uncertainties of experimental measurements.

TABLE 2.1 Reaction parameters for hydrogen oxidation kinetics (Burke et al., 2010).

			A	n	E_a	Reference
(1)	$H+O_2=O+OH$		1.04E+14	0.00	1.531E+04	Hong et al. (2011)
(2)	$O+H_2=H+OH$	Duplicate	3.82E+12	0.00	7.948E+03	Baulch et al. (2005)
		Duplicate	8.79E+14	0.00	1.917E+04	
(3)	$H_2+OH=H_2O+H$		2.16E+08	1.51	3.430E+03	Michael et al. (1988)
(4)	$OH+OH=O+H_2O$		3.34E+04	2.42	−1.930E+03	Baulch et al. (2005)
(5)	$H_2+M=H+H+M$		4.58E+19	−1.40	1.040E+05	Tsang et al. (1986)
	$\varepsilon_{H2}=2.5$, $\varepsilon_{H2O}=12.0$, $\varepsilon_{CO}=1.9$, $\varepsilon_{CO2}=3.8$, $\varepsilon_{Ar}=0.0$, $\varepsilon_{He}=0.0$					Li et al. (2004)
	$H_2+Ar=H+H+Ar$		5.84E+18	−1.10	1.040E+05	Tsang et al. (1986)
	$H_2+He=H+H+He$		5.84E+18	−1.10	1.040E+05	Li et al. (2004)
(6)	$O+O+M=O_2+M$		6.16E+15	−0.50	0.000E+00	Tsang et al. (1986)
	$\varepsilon_{H2}=2.5$, $\varepsilon_{H2O}=12.0$, $\varepsilon_{CO}=1.9$, $\varepsilon_{CO2}=3.8$, $\varepsilon_{Ar}=0.0$, $\varepsilon_{He}=0.0$					Li et al. (2004)
	$O+O+Ar=O_2+Ar$		1.89E+13	0.00	−1.790E+03	Tsang et al. (1986)
	$O+O+He=O_2+He$		1.89E+13	0.00	−1.790E+03	Li et al. (2004)
(7)	$O+H+M=OH+M$		4.71E+18	−1.00	0.000E+00	Tsang et al. (1986)
	$\varepsilon_{H2}=2.5$, $\varepsilon_{H2O}=12.0$, $\varepsilon_{CO}=1.9$, $\varepsilon_{CO2}=3.8$, $\varepsilon_{Ar}=0.75$, $\varepsilon_{He}=0.75$					Li et al. (2004)
(8)	$H_2O+M=H+OH+M$		6.06E+27	−3.32	1.208E+05	Srinivasan et al. (2006)
	$\varepsilon_{H2}=3.0$, $\varepsilon_{H2O}=0.0$, $\varepsilon_{CO}=1.9$, $\varepsilon_{CO2}=3.8$, $\varepsilon_{O2}=1.5$, $\varepsilon_{N2}=2.0$, $\varepsilon_{H2}=1.1$					See text
	$H_2O+H_2O=H+OH+H_2O$		1.01E+26	−2.44	1.202E+05	Srinivasan et al. (2006)
(9)	$H+O_2\ (+M)=HO_2\ (+M)^a$	k_∞	4.65E+12	0.44	0.000E+00	Troe et al. (2000)
		k_0	6.37E+20	−1.72	5.250E+02	Michael et al. (2002)
	$F_c=0.5$, $T^{***}=1.0E{-}30$, $T^{*}=1.0E+30$					Fernandes et al. (2008)
	$\varepsilon_{H2}=2.0$, $\varepsilon_{H2O}=14.0$, $\varepsilon_{CO}=1.9$, $\varepsilon_{CO2}=3.8$, $\varepsilon_{O2}=0.78$, $\varepsilon_{Ar}=0.67$, $\varepsilon_{He}=0.8$					See text

	$H+O_2$ (+M) = HO_2 (+M)[b]	k_∞	4.65E+12	0.44	0.000E+00	Troe et al. (2000)
		k_0	9.04E+19	−1.50	4.920E+02	Michael et al. (2002)
	F_c = 0.5, T^{***} = 1.0E–30, T^* = 1.0E+30					Fernandes et al. (2008)
	ε_{H2} = 3.0, ε_{H2O} = 21.0, ε_{CO} = 2.7, ε_{CO2} = 5.4, ε_{O2} = 1.1, ε_{He} = 1.2, ε_{N2} = 1.5					
(10)	$HO_2+H=H_2+O_2$		2.75E+06	2.09	−1.451E+03	Michael et al. (2000)
(11)	$HO_2+H=OH+OH$		7.08E+13	0.00	2.950E+02	Li et al. (2004)
(12)	$HO_2+O=O_2+OH$		2.85E+10	1.00	−7.239E+02	Fernández-Ramos et al. (2000)
(13)	$HO_2+OH=H_2O+O_2$		2.89E+13	0.00	−4.970E+02	Keyser et al. (1986)
(14)	$HO_2+HO_2=H_2O_2+O_2$	Duplicate	4.20E+14	0.00	1.200E+04	Hippler et al. (1990)
	$HO_2+HO_2=H_2O_2+O_2$	Duplicate	1.30E+11	0.00	−1.630E+03	
(15)	H_2O_2(+M) = OH+OH(+M)	k_∞	2.00E+12	0.90	4.875E+04	Troe et al. (2001)
		k_0	2.49E+24	−2.30	4.875E+04	Troe et al. (2001)
	F_c = 0.42, T^{***} = 1.0E–30, T^* = 1.0E+30					Troe et al. (2001)
	ε_{H2O} = 7.5, ε_{H2O2} = 7.7, ε_{CO2} = 1.6, ε_{O2} = 1.2, ε_{N2} = 1.5, ε_{He} = 0.65					Troe et al. (2001)
	ε_{H2} = 3.7, ε_{CO} = 2.8					
(16)	$H_2O_2+H=H_2O+OH$		2.41E+13	0.00	3.970E+03	Tsang et al. (1986)
(17)	$H_2O_2+H=HO_2+H_2$		4.82E+13	0.00	7.950E+03	Tsang et al. (1986)
(18)	$H_2O_2+O=OH+HO_2$		9.55E+06	2.00	3.970E+03	Tsang et al. (1986)
(19)	$H_2O_2+OH=HO_2+H_2O$	Duplicate	1.74E+12	0.00	3.180E+02	Hong et al. (2010)
		Duplicate	7.59E+13	0.00	7.270E+03	

Units are cm^3 *mol s cal K;* $k = AT^n\ exp(-E_a/RT)$.

2.3 Hydrogen combustion properties

2.3.1 Hydrogen flames

In this section, we will focus on discussing the difference between hydrogen flames with flames of other fuels. The underlying flame fundamentals, such as governing equations and heat/mass transfer models, can be found in references (Glassman et al., 2014).

Flame speed (S_L) is an important property that dictates the flame shape and flame stability characteristics, such as blow-off and flashback. Compared to its hydrocarbon counterparts, hydrogen has extremely high laminar flame speeds. At ambient conditions (298 K and 1 atm), the unstretched laminar flame speed of stoichiometric hydrogen/air mixture is approximately 210 cm/s. In contrast, the corresponding flame speeds of stoichiometric CH_4/air mixture and C_3H_8/air mixture are approximately 40 cm/s and 44 cm/s, respectively. Fig. 2.6 shows the relative flame speeds (at $\phi = 1$, 1 atm, T_u = room temperature) for H_2 and C_1–C_6 hydrocarbon fuels, normalized by propane flame speed as a reference flame speed, $S_{L,ref}$. The dominant reasons for such a difference in flame speed are the significantly larger thermal and mass diffusivities of hydrogen and the rapid H_2 oxidation kinetics compared to the relatively slow CO ➔ CO_2 step for hydrocarbons.

Hydrogen flame has a unique structure compared to its hydrocarbon counterparts. Figs. 2.7 and 2.8 show flame structures of hydrogen flame and methane flame as a comparison.

It can be seen that hydrogen flame is thicker (thicker heat release zone) than methane flame. However, the pre-heat zone of hydrogen flame is much thinner. Due to the large H atom concentration in hydrogen flame, extensive upstream H atom diffusion causes a sharp rise in HO_2, which reacts with H_2 fuel to form H atoms and H_2O_2. H_2O_2 is then dissociated into OH radicals immediately. Even when the temperature in the pre-heat zone is low, OH can still react with H_2 to form a large number of H atoms and H_2O to release a large amount of heat.

One surprising phenomenon is shown in Fig. 2.7 (left) is the increase of O_2 in the pre-heat zone. The increase in O_2 mole fraction (not in mass) owes to the fast diffusion of H_2 at the flame front.

The general trend of variation of flame speed with equivalence ratio follows the variation with flame temperature. Therefore, flame speeds of hydrocarbon/air mixtures peak slightly at the fuel-rich side. However, for hydrogen/air mixture, the maximum flame speed falls well on the fuel-rich side. This is owing to the excess hydrogen, which increases the thermal diffusivity of the mixture substantially. As shown in Fig. 2.9, the hydrogen/air mixture has a maximum flame speed of approximately 325 cm/sec near $\phi = 1.7$.

In the practical application of hydrogen combustion, an enriched oxygen environment might be desired. It is not difficult to imagine that flame speeds increase in general with the increase of oxygen content in the oxidizer, such as synthetic air. This is majorly due to the increase of flame temperature (therefore reaction rates) and potentially the change of diffusivities. Compared to the methane/air mixture, the flame speed increases by approximately a factor of 10 for the methane/oxygen mixture. For hydrogen, such an increase is about 3.5 times. The relative mild increase of flame speeds with oxygen concentration for hydrogen fuel is probably due to high radical concentrations in hydrogen combustion. So, the response of flame speeds to oxygen concentration (subsequently radical pool concentration) is relatively mild compared to that of hydrocarbon flames.

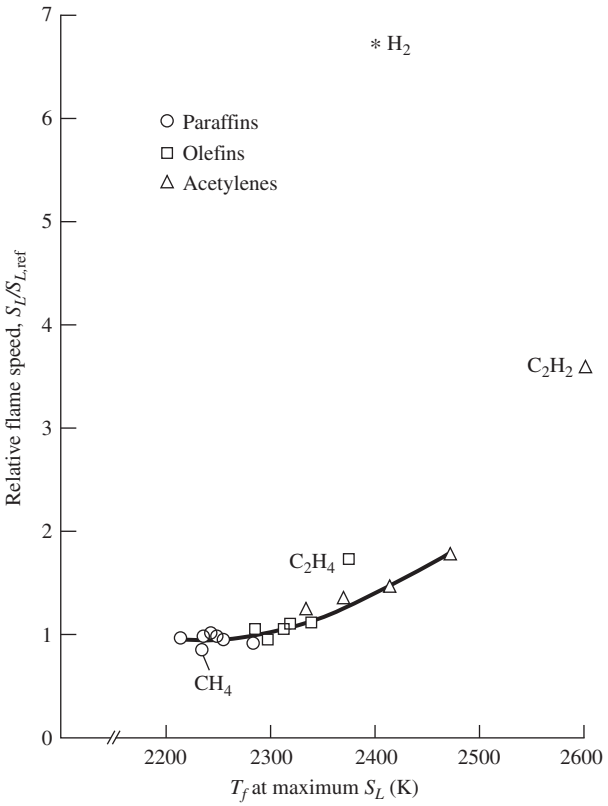

FIG. 2.6 Relative flame speeds for hydrogen and C_1–C_6 hydrocarbon fuels. *Adapted from Turns, S., 2011. An Introduction to Combustion: Concepts and Applications, third ed., McGraw-Hill Education. ISBN: 978-0073380193.*

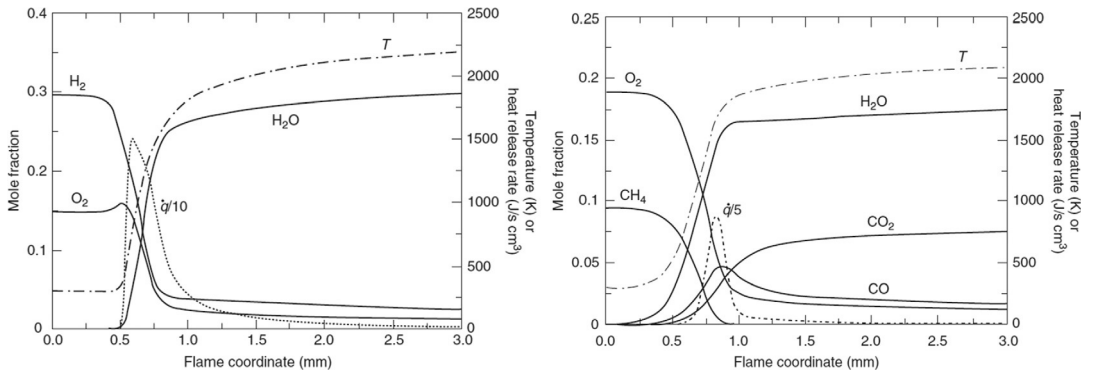

FIG. 2.7 Composition, temperature, and heat release rate profiles for a stoichiometric *(left)* H_2/air *(right)* CH_4/air laminar pre-mixed flame at 1 atm and $T_o = 298$ K. *Adapted from Glassman, I., Yetter, R.A., Glumac, N.G., 2014. Combustion. Academic Press.*

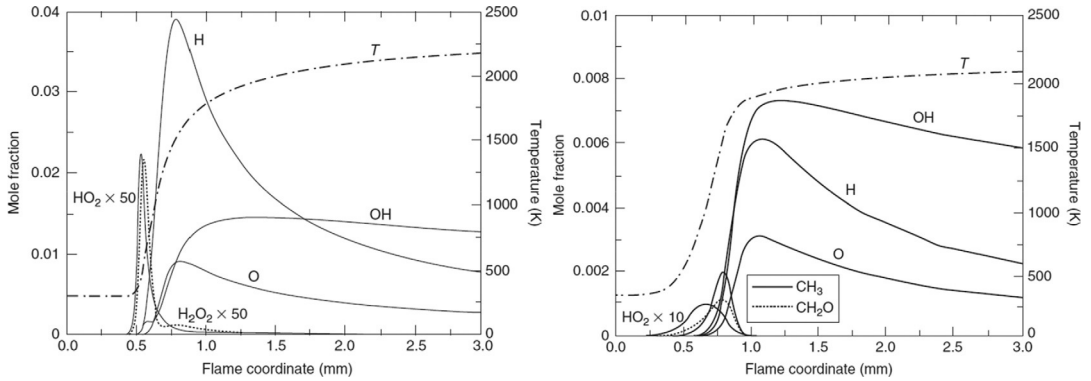

FIG. 2.8 Radical and temperature distribution of stoichiometric *(left)* H_2/air *(right)* CH_4/air laminar pre-mixed flame at 1 atm and $T_o = 298$ K. *Adapted from Glassman, I., Yetter, R.A., Glumac, N.G., 2014. Combustion. Academic Press.*

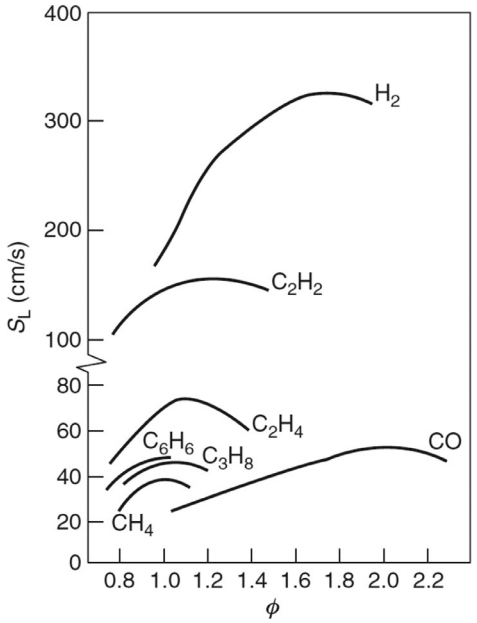

FIG. 2.9 General trend of laminar flame speeds with equivalence ratio for different fuel/air mixtures at $P = 1$, To = 298 K (Glassman et al., 2014).

2.3.2 Hydrogen ignition

For hydrogen fuel, there are typically two types of ignition, forced ignition, and auto-ignition (spontaneous ignition).

The most common form of forced ignition is probably spark ignition, which takes place in automotive engines. The spark deposits energy into a normally gaseous fuel/air mixture to elevate the mixture's temperature and produce a certain amount of radicals. Therefore, a concept of minimum ignition energy is introduced as a parameter to evaluate the ignitability of

fuels. The detailed mechanism of spark ignition is rather complex. The minimum energy is affected by several factors such as electrode spacing and geometries and mixture conditions that affect the generation of electrical discharge and heat transfer features. Most experimental investigations on the minimum ignition energy with electrode spacing provide the lowest values (Glassman et al., 2014), and the most commonly used electrode geometry is a metal rod. One interesting observation is that there appears to be a direct relationship between minimum ignition energy and the quenching distance (Glassman et al., 2014). Fig. 2.10 from (Calcote et al., 1952) shows the correlation of minimum spark ignition energy with quenching diameter of various stoichiometric fuel/air mixtures at 1 atm.

Another critical parameter to characterize the kinetics of fuel is autoignition delay. Autoignition of hydrogen can initiate an explosion reaction or sustained combustion based on the operating pressure and temperature conditions. The pressure and temperature can influence how the chain propagation and termination reactions compete. Domination of chain propagation reaction rates is undesirable, as it can lead to an explosion that is difficult to control. A balance between rates of propagation and termination reactions can favor stable combustion. Thus, investigation of autoignition combustion and explosion characteristics is critical. Seven important parameters that contribute to the autoignition of H_2 are: (1) pressure of the mixture, (2) initial temperature of the mixture, (3) equivalence ratio, (4) the percentage of diluent in the mixture, (5) degree of mixing, (6) fuel blend, and (7) shear strain or timescale of the flow. Theoretically, pressure increases the collision probability of molecules and increases the autoignition nature of a mixture at a given temperature, equivalence ratio, and other mixture conditions. However, in reality, autoignition has a complex dependency with pressure based on the fuel blend. For example, as shown in Fig. 2.11, the ignition delay of CH_4 or natural gas (NG) decreases with pressure, but pure hydrogen shows a peculiar trend (blue line) with pressure (Brower et al., 2013). It must be noted that Fig. 2.11 is the modeled data at 1100 K by Brower et al. (2013). In addition, trends in Fig. 2.11 might vary based on the initial temperatures. Below a certain temperature, the mixture may not autoignite irrespective of either pressure or fuel composition.

Hydrogen autoignition has been extensively investigated in the past. Experimental data on hydrogen autoignition delays were obtained up to supercritical conditions (above 200 atm) (Karimi et al., 2021; Shao et al., 2019), and the performance of most kinetic models at high-temperature conditions (above 1200 K) are satisfactory. However, the situation becomes complicated at lower temperature conditions (below 1000 K).

Many researchers have hypothesized that inhomogeneities (impurities, particles, and facility surfaces) can influence the autoignition of high hydrogen content (HHC) fuels at low temperatures (in the pre-mixer, $T \sim 600$–1000 K) and thus can affect the flashback (Wang et al., 2003). In shock tube studies, contamination on the experimental surface reduced H_2 ignition delay time compared to a clean tube (Wang et al., 2003). Surfaces could promote chemical induction by catalytic enhancements in H_2 systems (Chaos and Dryer, 2008). In addition, it was observed that particles (present in gases) as small as 0.01 μm were responsible for non-uniform, accelerated ignition, and also that invisible particulate matter deposits on the wall chamber (even in fuel-lean cases) acted as a particle reservoir. This interaction was thought to be due to the catalytic oxidation of fuel on the particle surface. It was found that experiments with increasing hydrogen content were always controlled by particle ignition. The gas-phase produced radicals can recombine on the metal surface (Reinke et al., 2005;

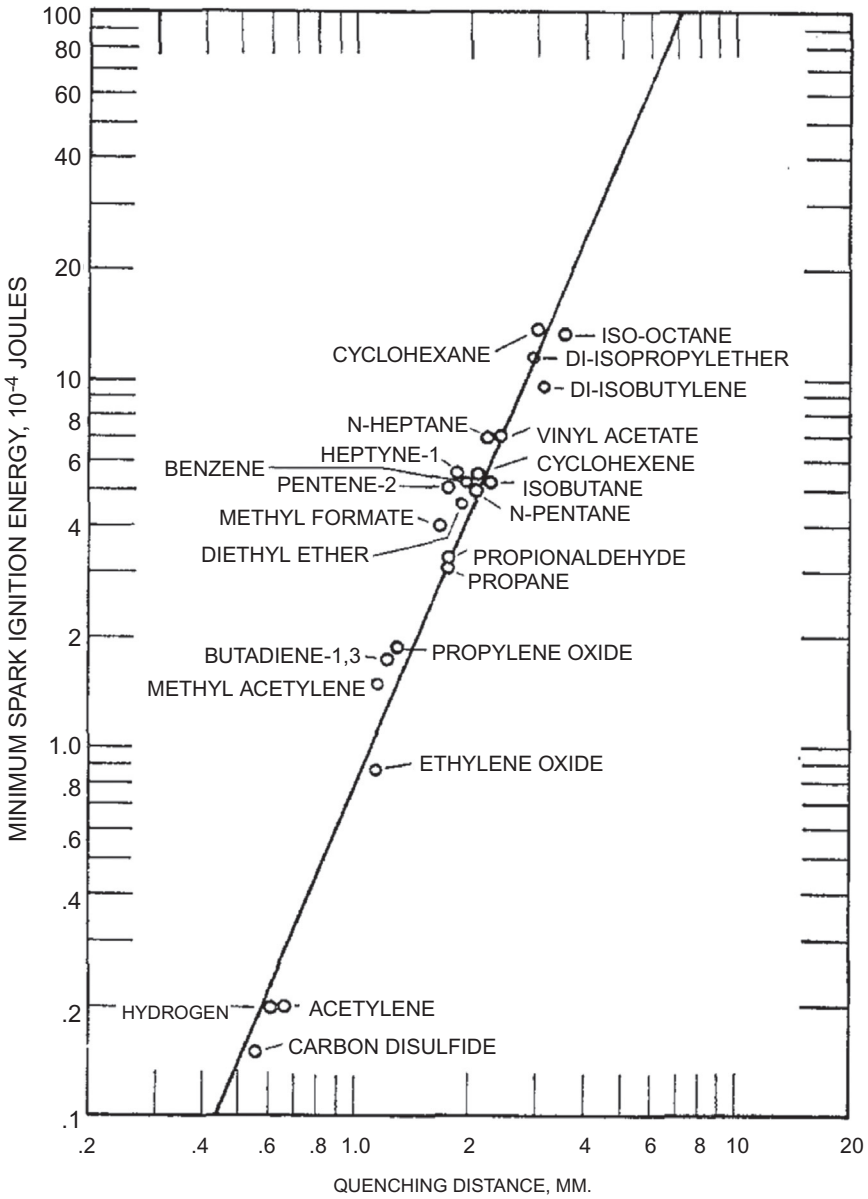

FIG. 2.10 Correlation of minimum spark ignition energy with quenching distance, $\phi = 1$, $P = 1$ atm. *Adapted from Calcote, H.F., Gregory, Jr. C.A., Barnett, C.M., Gilmer, R.B., 1952. Ind. Eng. Chem. 44, 2656.*

Mantzaras et al., 2009), and the surface chemistry does play a role on the lower (first) explosion limit because this limit refers to very low subatmospheric pressures (~1/100 atm), which is affected by the vessel surface. Very recently, the effects of pre-ignition energy release on H_2-O_2 mixtures were explored in a shock tube with the aid of high-speed imaging and

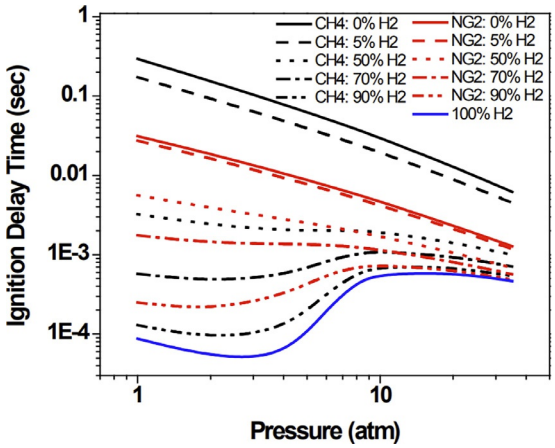

FIG. 2.11 Autoignition delay dependency of CH_4, NG, and H_2 fuels on pressure (Brower et al., 2013).

conventional pressure and emission diagnostics by Ninnemann et al. (2018). Ignition delay times and time-resolved camera image sequences were taken behind the reflected shockwaves for two hydrogen mixtures. Experiments were performed in both a clean and dirty shock tube facility; however, no deviations in ignition delay times between the two types of tests were apparent. The high-concentration mixture ($15\%H_2\backslash 18\%O_2\backslash Ar$) experienced energy releases in the form of deflagration flames followed by local detonations at temperatures <1000 K. The lower concentration mixture pressure time-histories exhibited no signs of pre-ignition energy releases. Further investigations are still needed regarding the ignition features of hydrogen at low-temperature conditions.

NO has a catalytic effect on H_2 autoignition (Ombrello et al., 2008). The catalytic enhancement pathway is from the reaction with relatively inactive HO_2 radicals via reactions

$$HO_2 + NO \rightarrow OH + NO_2 \quad \text{(xxi)}$$

$$H + NO_2 \rightarrow OH + NO \quad \text{(xxii)}$$

NOs existence in the mixture could convert HO_2 into more reactive radicals, OH, therefore accelerating the ignition process. It was shown that a NO addition could significantly reduce the autoignition temperature of H_2 in a diffusion counterflow system at atmospheric pressure conditions (Ombrello et al., 2008). The decrease of H_2/air mixture autoignition delays with NO (and NO_2) additions was also reported (Snyder et al., 1965).

A recent study from Mathieu et al. (2013) showed the effect of a NO_2 addition on H_2 autoignition is sensitive to both pressures and NO_2 concentrations, and the dependence on equivalence ratio is negligible. Fig. 2.12 shows the experimentally measured autoignition delays of the $H_2/O_2/Ar$ mixture with and without NO_2 addition. Their shock tube autoignition delay data showed that the addition of NO_2 up to 400 ppm was promoting autoignitions above 1.5 atm via reactions (xxi) and (xxii). Moreover, such enhancement is more significant at lower temperature conditions. However, a higher concentration of

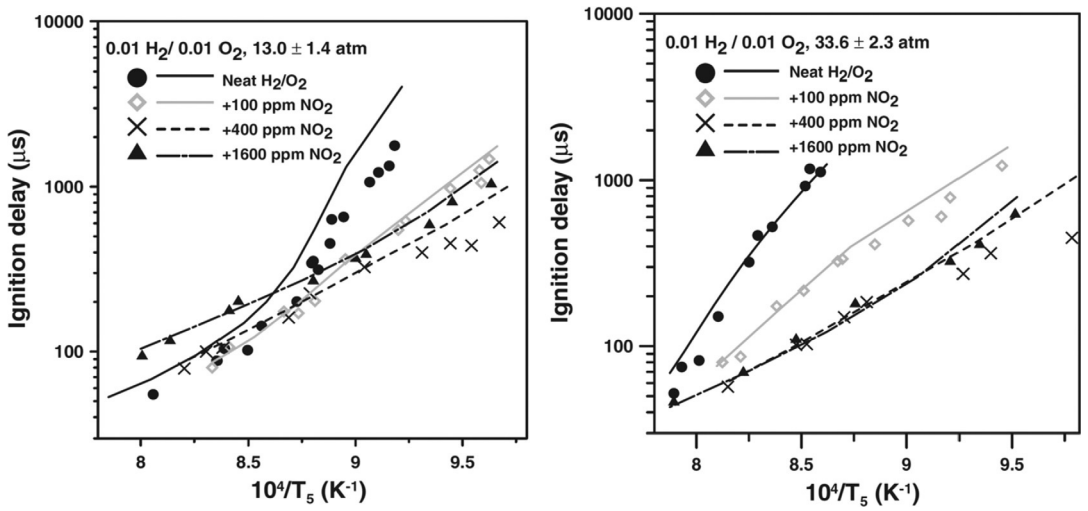

FIG. 2.12 Effect of NO_2 concentration on auto-ignition delay for H_2O_2/Ar mixtures at *(left)* approximately 13 atm and *(right)* approximately 33 atm; symbols are from experiments and lines are from modeling (Mathieu et al., 2013).

NO_2 addition, for the case of 1600 ppm, could inhibit autoignition (longer autoignition delays). This is owing to the promotion of a chain propagating reaction $OH + H_2 \rightarrow H + H_2O$ by a high, NO_2 concentration rather than promoting the chain branching reaction $H + O_2 \rightarrow OH + O$ (NO_2 consumes H radicals).

From the discussion, we can see that the effect of NO/NO_2 on hydrogen ignition still requires further investigation as the trend is non-linear. It is also worth noting that NO/NO_2 does not affect the flame properties since the radical pool is already built up in a flame but does not exist before ignition occurs.

References

Atkinson, A., et al., 2004. Evaluated kinetic and photochemical data for atmospheric chemistry: volume I-gas phase reactions of O_x, HO_x, NO_x and SO_x species. Atmos. Chem. Phys. 4 (6), 1461–1738.

Barnett, H.C., Hibbard, R.R., 1958. Basic Considerations in the Combustion of Hydrocarbon Fuels with Air, 1300. US Government Printing Office.

Baulch, D.L., Bowman, C.T., Cobos, C.J., Cox, R.A., Just, T., Kerr, J.A., Pilling, M.J., Stocker, D., Troe, J., Tsang, W., Walker, R.W., Warnatz, J., 2005. Evaluated kinetic data for combustion modeling: supplement II. J. Phys. Chem. Ref. Data, 34, 757–1397.

Brower, M., et al., 2013. Ignition delay time and laminar flame speed calculations for natural gas/hydrogen blends at elevated pressures. J. Eng. Gas Turbines Power 135, 2.

Burke, M.P., Chaos, M., Dryer, F.L., Ju, Y., 2010. Negative pressure dependence of mass burning rates of $H_2/CO/O_2$/diluent flames at low flame temperatures. Combust. Flame 157 (4), 618–631.

Burke, M.P., Chaos, M., Ju, Y., Dryer, F.L., Klippenstein, S.J., 2021. Comprehensive H_2/O_2 kinetic model for high-pressure combustion. Int. J. Chem. Kinet. 44 (7), 444–474.

Burke, M.P., Klippenstein, S.J., 2017. Ephemeral collision complexes mediate chemically termolecular transformations that affect system chemistry. Nat. Chem. 9 (11), 1078–1082.

Calcote, H.F., Gregory Jr., C.A., Barnett, C.M., Gilmer, R.B., 1952. Spark ignition. Effect of molecular structure. Ind. Eng. Chem. 44, 2656.

Chaos, M., Dryer, F.L., 2008. Syngas combustion kinetics and applications. Combust. Sci. Technol. 180 (6), 1053–1096.

Colonna, G.R., 2010. Fire Protection Guide to Hazardous Materials: 117-81-7. National Fire Protection Association Location, Quincy, MA.
Davis, S.G., Joshi, A.V., Wang, H., Egolfopoulos, F., 2005. An optimized kinetic model of H_2/CO combustion. Proc. Combust. Inst. 30 (1), 1283–1291.
Fernandes, R.X., Luther, K., Troe, J., Ushakov, V.G., 2008. Experimental and modelling study of the recombination reaction H + O_2 (+M) → HO_2 (+M) between 300 and 900 K, 1.5 and 950 bar, and in the bath gases M = He, Ar, and N_2. Phys. Chem. Chem. Phys. 10, 4313–4321.
Fernández-Ramos, A., Varandas, A.J.C., 2002. A VTST study of the H + O_3 and O + HO_2 reactions using a six-dimensional DMBE potential energy surface for ground state HO_3. J. Phys. Chem. A 106, 4077–4083.
Glassman, I., Yetter, R.A., Glumac, N.G., 2014. Combustion. Academic Press.
Haynes, W.M., 2014. CRC Handbook of Chemistry and Physics. CRC Press.
Hippler, H., Troe, J., Willner, J., 1990. Shock wave study of the reaction HO_2 + HO_2 → H_2O_2 + O_2: confirmation of a rate constant minimum near 700 K. J. Chem. Phys. 93, 1755–1760.
Hong, Z., Cook, R.D., Davidson, D.F., Hanson, R.K., 2010. A shock tube study of OH + H_2O_2 → H_2O + HO_2 and H_2O_2 + M → 2OH + M using laser absorption of H_2O and OH. J. Phys. Chem. A 114, 5718–5727.
Hong, Z., Davidson, D.F., Barbour, E.A., Hanson, R.K., 2011. A new shock tube study of the H + O_2 → OH + O reaction rate using tunable diode laser absorption of H_2O near 2.5 μm. Proc. Combust. Inst. 33, 309–316.
Hong, Z., Davidson, D.F., Hanson, R.K., 2011. An improved H_2/O_2 mechanism based on recent shock tube/laser absorption measurements. Combust. Flame 158 (4), 633–644.
Jasper, A.W., Kamarchik, E., Miller, J.A., Klippenstein, S.J., 2014. First-principles binary diffusion coefficients for H, H_2, and four normal alkanes+ N_2. J. Chem. Phys. 141 (12), 124313.
Karimi, M., Ochs, B., Sun, W., Ranjan, D., 2021. High pressure ignition delay times of H_2/CO mixture in carbon dioxide and argon diluent. Proc. Combust. Inst. 38 (1), 251–260.
Kéromnès, A., et al., 2013. An experimental and detailed chemical kinetic modeling study of hydrogen and syngas mixture oxidation at elevated pressures. Combust. Flame 160 (6), 995–1011.
Keyser, L.F., 1986. Absolute rate constant and branching fractions for the atomic hydrogen + hydroperoxyl radical reaction from 245 to 300 K. J. Phys. Chem. 90, 2994–3003.
Klippenstein, S.J., 2017. From theoretical reaction dynamics to chemical modeling of combustion. Proc. Combust. Inst. 36 (1), 77–111.
Konnov, A.A., 2008. Remaining uncertainties in the kinetic mechanism of hydrogen combustion. Combust. Flame 152 (4), 507–528.
Konnov, A.A., 2019. Yet another kinetic mechanism for hydrogen combustion. Combust. Flame 203, 14–22.
Lewis, B., von Elbe, G., 1987. Combustion, Flames and Explosions of Gases, third ed. Academic Press.
Li, J., Zhao, Z., Kazakov, A., Dryer, F.L., 2004. An updated comprehensive kinetic model of hydrogen combustion. Int. J. Chem. Kinet. 36 (10), 566–575.
Mantzaras, J., Bombach, R., Schaeren, R., 2009. Hetero-/homogeneous combustion of hydrogen/air mixtures over platinum at pressures up to 10 bar. Proc. Combust. Inst. 32 (2), 1937–1945.
Mathieu, O., Levacque, A., Petersen, E.L., 2013. Effects of NO_2 addition on hydrogen ignition behind reflected shock waves. Proc. Combust. Inst. 34 (1), 633–640.
Michael, J.V., Su, M.-C., Sutherland, J.W., Carroll, J.J., Wagner, A.F., 2002. Rate constants for H + O_2 + M → HO_2 + M in seven bath gases. J. Phys. Chem. A 106, 5297–5313.
Michael, J.V., Sutherland, J.W., 1988. Rate constants for the reactions of hydrogen atom with water and hydroxyl with hydrogen by the flash photolysis-shock tube technique over the temperature range 1246–2297 K. J. Phys. Chem. 92, 3853–3857.
Michael, J.V., Sutherland, J.W., Harding, L.B., Wagner, A.F., 2000. Initiation in H_2/O_2: rate constants for H_2 + O_2 → H + HO_2 at high temperature. Proc. Combust. Inst. 28, 1471–1478.
Ninnemann, E., et al., 2018. New insights into the shock tube ignition of H_2/O_2 at low to moderate temperatures using high-speed end-wall imaging. Combust. Flame 187, 11–21.
ÓConaire, M., Curran, H.J., Simmie, J.M., Pitz, W.J., Westbrook, C.K., 2004. A comprehensive modeling study of hydrogen oxidation. Int. J. Chem. Kinet. 36 (11), 603–622.
Okino, T., et al., 2017. Ultraviolet and visible spectral imaging of hydrogen flames using an organic photoconductive film CMOS imager. In: Proceedings of the International Image Sensor Workshop, pp. 188–191.
Ombrello, T., Ju, Y., Fridman, A., 2008. Kinetic ignition enhancement of diffusion flames by nonequilibrium magnetic gliding arc plasma. AIAA J. 46 (10), 2424–2433.

Pelucchi, M., Cavallotti, C., Cuoci, A., Faravelli, T., Frassoldati, A., Ranzi, E., 2019. Detailed kinetics of substituted phenolic species in pyrolysis bio-oils. React. Chem. Eng. 4 (3), 490–506.
Reinke, M., Mantzaras, J., Schaeren, R., Bombach, R., Inauen, A., Schenker, S., 2005. Homogeneous ignition of CH_4/air and H_2O and CO_2-diluted CH_4/O_2 mixtures over Pt; an experimental and numerical investigation at pressures up to 16 bar. Proc. Combust. Inst. 30 (2), 2519–2527.
Saxena, P., Williams, F.A., 2006. Testing a small detailed chemical-kinetic mechanism for the combustion of hydrogen and carbon monoxide. Combust. Flame 145 (1–2), 316–323.
Schefer, R.W., Kulatilaka, W.D., Patterson, B.D., Settersten, T.B., 2009. Visible emission of hydrogen flames. Combust. Flame 156 (6), 1234–1241.
Schefer, R.W., Smith, T.D., Marek, C.J., 2002. Evaluation of NASA Lean Premixed Hydrogen Burner, SAND2002-8609. Sandia National Laboratories, Livermore, CA.
Shao, J., Choudhary, R., Davidson, D.F., Hanson, R.K., Barak, S., Vasu, S., 2019. Ignition delay times of methane and hydrogen highly diluted in carbon dioxide at high pressures up to 300 atm. Proc. Combust. Inst. 37 (4), 4555–4562.
Smith, G.P., et al., 2008. GRI-3.0 Mechanism.
Snyder, A.D., Skinner, G.B., Robertson, J., Zanders, D.L., 1965. Shock Tube Studies of Fuel-Air Ignition Characteristics. Monsanto Research Corp, Dayton, OH.
Srinivasan, N.K., Michael, J.V., 2006. The thermal decomposition of water. Int. J. Chem. Kinet. 38, 211–219.
Sun, H., Yang, S.I., Jomaas, G., Law, C.K., 2007. High-pressure laminar flame speeds and kinetic modeling of carbon monoxide/hydrogen combustion. Proc. Combust. Inst. 31 (1), 439–446.
Troe, J., 2000. Detailed modeling of the temperature and pressure dependence of the reaction $H + O_2$ (+M) → HO_2 (+M). Proc. Combust. Inst. 28, 1463–1469.
Troe, J., 2001. The thermal dissociation/recombination reaction of hydrogen peroxide H_2O_2 (+M) ⇔ 2OH (+M) III: analysis and representation of the temperature and pressure dependence over wide ranges. Combust. Flame 158, 594–601.
Tsang, W., Hampson, R.F., 1986. Chemical kinetic data base for combustion chemistry. Part I. Methane and related compounds. J. Phys. Chem. Ref. Data 15, 1087–1222.
U. S. C. Guard, 1999. Chemical Hazard Response Information System (CHRIS)-Hazardous Chemical Data. Command. Instr., 16465.
Varga, T., et al., 2015. Optimization of a hydrogen combustion mechanism using both direct and indirect measurements. Proc. Combust. Inst. 35 (1), 589–596.
Wang, B.L., Olivier, H., Grönig, H., 2003. Ignition of shock-heated H_2-air-steam mixtures. Combust. Flame 133 (1–2), 93–106.
Wang, H., et al., 2007. USC Mech Version II. High-Temperature Combustion Reaction Model of H_2/CO/C1-C4 Compounds.
Westbrook, C.K., Dryer, F.L., 1984. Chemical kinetic modeling of hydrocarbon combustion. Prog. Energy Combust. Sci. 10 (1), 1–57.
Wiberg, E., Wiberg, N., Holleman, A.F., 2001. Inorganic Chemistry. Academic Press.
Zabetakis, M.G., 1965. Flammability Characteristics of Combustible Gases and Vapors; US Bureau of Mines Bulletin 627.